Electrocatalytic activity towards oxygen reduction reaction of laminar nanocomposite $LaNb_2O_7/Co^{III}TMPyP$ prepared via the exfoliation/restacking method

Jiasheng Xu[1], Binbin Pan[1], Jinpeng Li[1], Xiaobo Zhang[1], Mengjun Wang[1], Zhiwei Tong[1,2,3] ✉

[1]*School of Chemical Engineering, Huaihai Institute of Technology, Lianyungang 222005, People's Republic of China*
[2]*Country College of Chemistry and Chemical Engineering, Lanzhou University, Lanzhou 730000, People's Republic of China*
[3]*SORST, Japan Science and Technology Agency (JST), Kawaguchi Center Building 4-1-8, Kawaguchi-shi, Saitama 332-0012, Japan*
✉ *E-mail: zhiweitong575@hotmail.com*

Published in Micro & Nano Letters; Received on 31st January 2017; Revised on 3rd May 2017; Accepted on 23rd May 2017

The laminar lanthanum niobate $KLaNb_2O_7$ with perovskite structure was intercalated with cationic cobalt (III) tetrakis-5, 10, 15, and 20-(N-methyl-4-pyridyl) porphyrin using the exfoliation/restacking method. The as-prepared material was characterised by several analytic methods including X-ray diffraction, scanning electron microscopy, transmission electron microscopy, and infrared microscopy. The exfoliation/restacking process was monitored and proved by the change of zeta potential, and the cyclic voltammetry measurements of $LaNb_2O_7/Co^{III}TMPyP$ nanocomposite demonstrated excellent electrocatalytic activity towards oxygen reduction reaction.

1. Introduction: With the increasing environmental concern caused by the fossil fuel combustion, alternative clean energy solutions such as fuel cells and metal-air batteries are investigated intensively [1]. The oxygen reduction reaction (ORR) in these systems needs efficient electrocatalysts. Noble metal and noble metal oxides, which exhibit excellent electrocatalytic activity for ORR, have limited applications in the field of renewable energy sources because of the storage and cost issues [2, 3]. The state-of-the-art catalyst Pt/C for ORR has reduced the cost of Pt and enhanced the activity of Pt nanoparticles, but it is quite difficult to gain both high surface area and the desired highly active facets on their surfaces [4, 5]. Hence, stable and efficient non-metal catalysts for ORR have attracted great interests in the field [6–10]. Metalloporphyrins, especially cobalt porphyrin, possess eminent catalytic properties towards ORR in the electrochemical system [11–14]. The cationic cobalt (III) tetrakis-5, 10, 15, 20-(N-methyl-4-pyridyl) porphyrin ($Co^{III}TMPyP$) has good electrocatalytic activity towards ORR [15]. However, metalloporphyrins are unstable in organic media and sensitive to the temperature and the pH of reaction environment. One strategy to improve the stability is to immobilise metalloporphyrins into the interlayer of host materials [16–20].

Several two-dimensional layered nanocomposites with perovskite structure have been reported extensively due to their unique structural properties and wide applications in the field of electronics, optics, catalysts, and electrochemistry [21–24]. The exfoliated nanosheets derived from the perovskites ($Ca_2Nb_3O_{10}^-$, $TiNbO_5^-$, $Nb_3O_8^-$) have gained increased attention in recent reports [25–28]. These nanosheets have unique functionalities with atomic or molecular thickness. In addition, they can be used as building blocks in electrostatic layer-by-layer (LBL) assembly [29]. As a typical D-J phase perovskite, the lanthanum potassium niobate $KLaNb_2O_7$ has been investigated considerably because of its good ion-exchange capability and intercalation properties [30–33]. However, to the best of our knowledge, there are few reports on the exfoliation of $KLaNb_2O_7$ in the field of intercalation [34].

Herein, the lamellar nanocomposite of $LaNb_2O_7/Co^{III}TMPyP$ was prepared via the exfoliation/restacking method and the electrocatalytic activity of the $LaNb_2O_7/Co^{III}TMPyP$ thin film was investigated in our work. The as-prepared material exhibits excellent electrocatalytic activity towards ORR.

2. Experiment: $KLaNb_2O_7$ was synthesised by sintering a stoichiometric mixture of K_2CO_3, La_2O_3, and Nb_2O_5 at 1423 K for 24 h [35]. The corresponding layered acidic material $HLaNb_2O_7$ was produced by three times of treating $KLaNb_2O_7$ in 6 M nitrate acid for 24 h at room temperature and then drying at 50°C for 24 h. For exfoliation procedure, $HLaNb_2O_7$ (0.3 g) was added into 10 wt% aqueous solution of TBA^+OH^- and 110 ml of deionised water under uniform stirring for 5 days at room temperature. Colloidal suspension of exfoliated $LaNb_2O_7^-$ nanosheets was obtained by centrifuge. $LaNb_2O_7/Co^{III}TMPyP$ intercalation composite was fabricated by adding 1 mM cobalt porphyrin aqueous solution into the stable $LaNb_2O_7^-$ colloidal suspension (shown in Fig. 1). The solid deposit of $LaNb_2O_7/Co^{III}TMPyP$ was then separated by centrifuging the mixture at 8000 rpm and washing with deionised water for three times. The final precipitate was dried in a vacuum oven at 50°C for 24 h.

X-ray diffraction (XRD) patterns were obtained via a RINT 2000 diffractometer (Rigaku) with the monochromatised Cu Kα radiation ($\lambda = 1.5406$ Å) and a scan ranges from 2° to 70° 2θ at 40 mA and 40 kV. A JSM-5600 apparatus (JEOL) and a JEM-2010 instrument (JEOL) were employed to collect images of scanning electron microscopy (SEM) for the Au-coated samples and high-resolution transmission electron microscopy, respectively. Fourier transform infrared (FTIR) spectroscopies were recorded on a Shimazu FTIR-8400S spectrometer with KBr pellets. The zeta potentials of the mixture of $LaNb_2O_7^-$ nanosheets colloidal dispersion and cobalt porphyrin aqueous solution were tested via the Malvern Zetasizer Nano Instrument.

The electrochemical measurements were performed on a CHI660C electrochemical workstation at room temperature in a three-electrode test cell with a saturated calomel electrode as the reference electrode and a platinum wire as the counter electrode. The working electrode was prepared by dropping 7 µl $LaNb_2O_7/Co^{III}TMPyP$ homogeneous-dispersed aqueous suspension (mass concentration, 2 mg/ml) on a bare glass carbon electrode (GCE) and dried for 24 h. The electrochemical measurement of cyclic voltammetry (CV) is used to test the electro-catalysis towards ORR of the as-prepared nanocomposite.

3. Result and discussion: The XRD patterns of $KLaNb_2O_7$, $HLaNb_2O_7$, and $LaNb_2O_7/Co^{III}TMPyP$ are shown in Fig. 2. The interlayer space of lanthanum niobate expands from 1.070

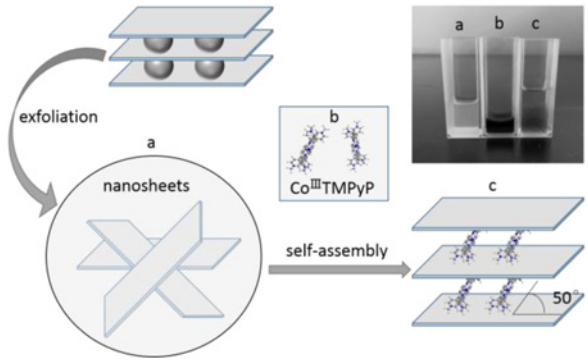

Fig. 1 *Self-assembly of $LaNb_2O_7^-$ sheets and cobalt porphyrin*

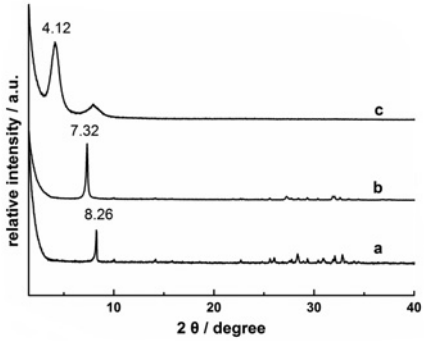

Fig. 2 *X-ray diffraction patterns of*
a $KLaNb_2O_7$
b $HLaNb_2O_7$
c $LaNb_2O_7/Co^{III}TMPyP$

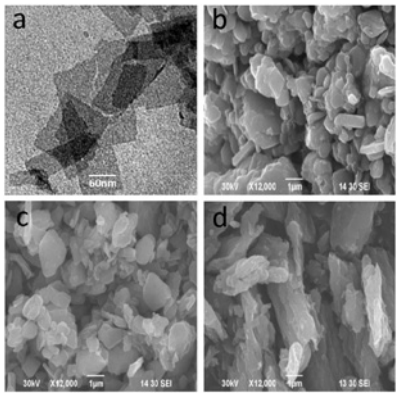

Fig. 3 *TEM and SEM images*
a TEM image of $LaNb_2O_7^-$ nanosheets
b SEM image of $KLaNb_2O_7$
c SEM image of $HLaNb_2O_7$
d SEM image of $LaNb_2O_7/Co^{III}TMPyP$ composite

to 1.207 nm after protonation. The interlayer space of the composite increases to 2.143 nm due to the much larger molecular dimension of $Co^{III}TMPyP$ (1.8×1.8 nm^2) [36] than that of the H_3O^+ ion. In consideration of the layer thickness of $LaNb_2O_7^-$ sheets (0.75 nm) [37], the calculated angle of the $Co^{III}TMPyP$ molecular surface towards the $LaNb_2O_7^-$ layer is around 50°. The transmission electron microscopy (TEM) image in Fig. 3*a* demonstrates the appearance of $LaNb_2O_7^-$ nanosheets and the successful exfoliation of $HLaNb_2O_7$. The SEM images of $KLaNb_2O_7$, $HLaNb_2O_7$, and $LaNb_2O_7/Co^{III}TMPyP$ nanocomposite are shown in Figs. 3*b–d*, respectively. It is apparent that the resulting product

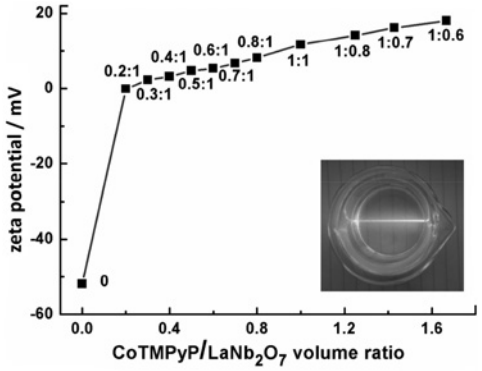

Fig. 4 *Relationship of the zeta potential and the ratio volume of $Co^{III}TMPyP/LaNb_2O_7$. Inset: the Tyndall phenomenon of the colloidal suspension (ratio = 0)*

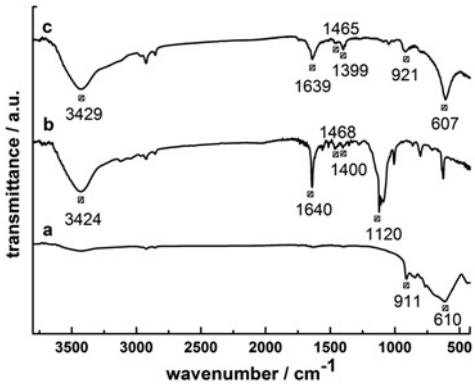

Fig. 5 *FTIR spectra of*
a $KLaNb_2O_7$
b $Co^{III}TMPyP$
c $Co^{III}TMPyP/LaNb_2O_7$

$LaNb_2O_7/Co^{III}TMPyP$ still maintains the layered structure of the parent material $KLaNb_2O_7$.

The relationship curve between the zeta potential and the $Co^{III}TMPyP/LaNb_2O_7$ volume ratio is shown in Fig. 4. The zeta potential of exfoliated $LaNb_2O_7^-$ nanosheets colloidal dispersion was –51.9 mV, the inset shows the Tyndall phenomenon in the colloidal solution of $LaNb_2O_7^-$ nanosheets. The zeta potential of the mixture with different $Co^{III}TMPyP/LaNb_2O_7$ volume ratio has been measured and the zeta potential value increases with the amount of $Co^{III}TMPyP$ aqueous solution added into $LaNb_2O_7^-$ colloidal suspension increases. Moreover, the zeta potential is ~0 mV when the $Co^{III}TMPyP/LaNb_2O_7$ volume ratio is 0.2.

The FTIR spectra of $KLaNb_2O_7$, $Co^{III}TMPyP$, and $Co^{III}TMPyP/LaNb_2O_7$ are shown in Fig. 5. Absorption peaks at 911 and 610 cm^{-1} are assigned to the Nb–O stretching vibration of $KLaNb_2O_7$ in Fig. 5*a*, while the peaks at 1640, 1468, 1400 cm^{-1} are ascribed to the C=N and C=C stretching vibrations of the porphyrin rings in Fig. 5*b*. It is clearly observed in Fig. 5*c* that the characteristic absorption peaks of $KLaNb_2O_7$ host compound and $Co^{III}TMPyP$ guest molecules appear in the infrared absorption spectra of $Co^{III}TMPyP/LaNb_2O_7$ composite, which proves the successful intercalation of $Co^{III}TMPyP$ molecules into the interlayer of the composite material.

Fig. 6 shows the CV results of the ORR on bare GCE, $KLaNb_2O_7$ modified GCE, $LaNb_2O_7/Co^{III}TMPyP$ modified GCE, and the $Co^{III}TMPyP$ aqueous solution in a 0.2 M O_2-saturated neutral phosphate buffer solution (PBS) with a scan rate of 100 mV s^{-1}. Apparently, the reduction peak potential of the $LaNb_2O_7/Co^{III}TMPyP$ nanocomposite modified GCE (–0.199 V) is 475 mV

doi: 10.1049/mnl.2016.0813

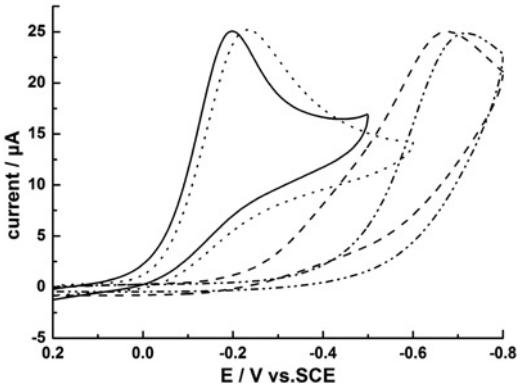

Fig. 6 *CV curves of $KLaNb_2O_7$ modified GCE (dotted line), $Co^{III}TMPyP$ aqueous solution (dash dot line), $LaNb_2O_7/Co^{III}TMPyP$ modified GCE (solid line), and bare GCE (dash line) in O_2-saturated 0.2 M PBS solution (pH = 7.0) at a scan rate of 100 mV s^{-1}*

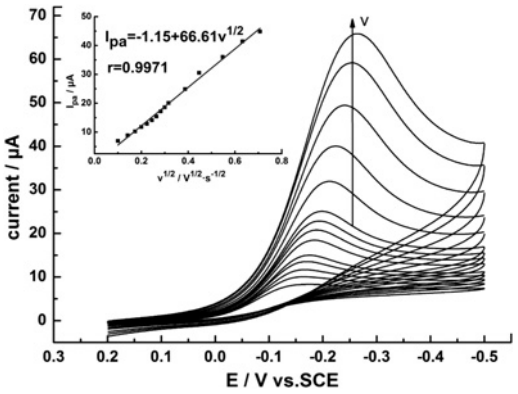

Fig. 7 *CV curves of $LaNb_2O_7/Co^{III}TMPyP$ modified GCE in O_2-saturated 0.2 M PBS solution (pH = 7.0) at scan rates of 20, 30, 40, 50, 60, 70, 80, 90, 100, 150, 200, 300, 400, 500 mV s^{-1} from inner to outer. Inset: relationship of I_{pa} and the square root of v*

higher than that of the bare GCE (–0.674 V), indicating that the $LaNb_2O_7/Co^{III}TMPyP$ intercalated composite exhibits excellent electrocatalytic activity towards ORR. The reduction peak potential of the $Co^{III}TMPyP$ aqueous solution is –0.233 V and that of $KLaNb_2O_7$ modified GCE is similar to bare GCE, suggesting that the $Co^{III}TMPyP$ molecule is the main active site. Furthermore, this film-modified GCE shows higher ORR current than the commercially available Pt/C electrode, indicating better electrocatalytic activity towards ORR [38].

As shown in Fig. 7, with the increase of scan rate, the reduction peak current increases gradually and the reduction peak potential shifts towards negative potentials accordingly. This can be attributed to the irreversibility of the ORR. The inset diagram in Fig. 7 exhibits a good linear relationship between the reduction peak current and the square root of v, and the linear equation is: $I\ (\mu A) = -1.15 + 66.61v^{1/2}$ ($V^{1/2}\ s^{-1/2}$) ($r = 0.9971$), indicating that the irreversible progress of ORR on the surface of $LaNb_2O_7/Co^{III}TMPyP$ modified GCE is controlled by the O_2 diffusion process. The relationship between the peak current and the scan rate can be demonstrated as the following equations [39]:

$$I_p = 0.4958nFAC_0\left(\frac{\alpha n_\alpha F}{RT}\right)^{1/2} v^{1/2}D_0^{1/2} \quad (1)$$

$$\Delta E_p = \frac{1.15RT}{\alpha n_\alpha F} \quad (2)$$

Where the known parameters are: A is the surface area of the electrode, F is the Faraday constant ($F = 96485.33$ C mol^{-1}), C_0 is the bulk concentration ($C_0 = 1.2$ mM, O_2-saturated), D_0 is the O_2 diffusion coefficient ($D_0 = 1.7 \times 10^{-5}$ $cm^2\ s^{-1}$), v is the scan rate ($v = 50$ mV s^{-1}), and ΔE_p is the peak separation when the scan rate increases ten-fold ($\Delta E_p = 88$ mV, from 50 mV s^{-1} to 500 mV s^{-1}). Therefore, the number of transferred electrons here is calculated as 1.92, implying that oxygen is reduced to H_2O_2 with a 2-electron process on the surface of the electrode.

4. Conclusion: $LaNb_2O_7/Co^{III}TMPyP$ intercalation nanocomposite was successfully fabricated via the exfoliation/restacking method. The final product is characterised by various analytic techniques. The value of zeta potential approaches to zero when the volume ratio of the $LaNb_2O_7$ colloidal dispersion and the $Co^{III}TMPyP$ aqueous solution was around 0.2. The CV measurements indicated that the $LaNb_2O_7/Co^{III}TMPyP$ nanocomposite exhibits excellent electrocatalytic activity towards oxygen reduction and oxygen is reduced to H_2O_2 with a 2-electron process on the surface of the electrode. The promising application of the $LaNb_2O_7/Co^{III}TMPyP$ nanocomposite in the field of electrocatalytic materials is proposed.

5. Acknowledgments: This work was supported by National Natural Science Foundation of China (grant nos. 21401062, 21201070, 51202079), Natural Science Fund of Jiangsu Province (grant nos. BK20161294, BK20140447, BK20141247, and SBK201220654), University Science Research Project of Jiangsu Province (grant nos. 13KJB430005, 12KJD150001, and 15KJB430004), the Research Innovation Program for College Graduate Students of Jiangsu Province (grant no. KYLX16_1416), and 521 High-level Personnel Training Research Project of Lianyungang City (grant no. KK15041).

6 References

[1] Sun J., Yin H., Liu P., *ET AL.*: 'Molecular engineering of Ni–/Co–porphyrin multilayers on reduced graphene oxide sheets as bifunctional catalysts for oxygen evolution and oxygen reduction reactions', *Chem. Sci.*, 2016, **7**, (9), pp. 5640–5646

[2] Otero R., Calleja F., Garcıa-Suárez V.M., *ET AL.*: 'Tailoring surface electronic states via strain to control adsorption: O/Cu/Ru (0001)', *Surf. Sci.*, 2004, **550**, (1), pp. 65–72

[3] Aoun S.B., Dursun Z., Sotomura T., *ET AL.*: 'Effect of metal ad-layers on Au (111) electrodes on electrocatalytic reduction of oxygen in an alkaline solution', *Electrochem. Commun.*, 2004, **6**, (8), pp. 747–752

[4] Lim B., Jiang M., Camargo P.H., *ET AL.*: 'Pd–Pt bimetallic nanodendrites with high activity for oxygen reduction', *Science*, 2009, **324**, (5932), pp. 1302–1305

[5] Wang C., Daimon H., Onodera T., *ET AL.*: 'A general approach to the size-and shape-controlled synthesis of platinum nanoparticles and their catalytic reduction of oxygen', *Angew. Chem. Int. Ed.*, 2008, **47**, (19), pp. 3588–3591

[6] Xiong W., Du F., Liu Y., *ET AL.*: '3-D carbon nanotube structures used as high performance catalyst for oxygen reduction reaction', *J. Am. Chem. Soc.*, 2010, **132**, (45), pp. 15839–15841

[7] Jaouen F., Herranz J., Lefevre M., *ET AL.*: 'Cross-laboratory experimental study of non-noble-metal electrocatalysts for the oxygen reduction reaction', *ACS Appl. Mater. Interfaces*, 2009, **1**, (8), pp. 1623–1639

[8] Liang Y., Li Y., Wang H., *ET AL.*: 'Co_3O_4 nanocrystals on graphene as a synergistic catalyst for oxygen reduction reaction', *Nat. Mater.*, 2011, **10**, (10), pp. 780–786

[9] Yang Z., Yao Z., Li G., *ET AL.*: 'Sulfur-doped graphene as an efficient metal-free cathode catalyst for oxygen reduction', *ACS Nano*, 2011, **6**, (1), pp. 205–211

[10] Gong K., Du F., Xia Z., *ET AL.*: 'Nitrogen-doped carbon nanotube arrays with high electrocatalytic activity for oxygen reduction', *Science*, 2009, **323**, (5915), pp. 760–764

[11] Jasinski R.: 'A new fuel cell cathode catalyst', *Nature*, 1964, **201**, (4925), pp. 1212–1213

[12] Liu H., Zhang L., Zhang J., *ET AL.*: 'Electrocatalytic reduction of O_2 and H_2O_2 by adsorbed cobalt tetramethoxyphenyl porphyrin and its application for fuel cell cathodes', *J. Power Sources*, 2006, **161**, (2), pp. 743–752

[13] Morozan A., Campidelli S., Filoramo A., *ET AL.*: 'Catalytic activity of cobalt and iron phthalocyanines or porphyrins supported on different

carbon nanotubes towards oxygen reduction reaction', *Carbon*, 2011, **49**, (14), pp. 4839–4847
[14] Goubert-Renaudin S.N., Zhu X., Wieckowski A.: 'Synthesis and characterization of carbon-supported transition metal oxide nanoparticles-cobalt porphyrin as catalysts for electroreduction of oxygen in acids', *Electrochem. Commun.*, 2010, **12**, (11), pp. 1457–1461
[15] Okada T., Gokita M., Yuasa M., *ET AL.*: 'Oxygen reduction characteristics of heat-treated catalysts based on cobalt-porphyrin ion complexes', *J. Electrochem. Soc.*, 1998, **145**, (3), pp. 815–822
[16] Cowan D.A.: 'Thermophilic proteins: stability and function in aqueous and organic solvents', *Comp. Biochem. Physiol. A, Physiol.*, 1997, **118**, (3), pp. 429–438
[17] Birnbaum T., Hahn T., Martin C., *ET AL.*: 'Optical and magneto-optical properties of metal phthalocyanine and metal porphyrin thin films', *J. Phys. Condens. Matter*, 2014, **26**, (10), pp. 104201
[18] Ichiki T., Matsuo Y., Nakamura E.: 'Photostability of a dyad of magnesium porphyrin and fullerene and its application to photocurrent conversion', *Chem. Commun.*, 2013, **49**, (3), pp. 279–281
[19] Bizeto M.A., De Faria D.L.A., Constantino V.R.L.: 'Porphyrin intercalation into a layered niobate derived from $K_4Nb_6O_{17}$', *J. Mater. Sci.*, 2002, **37**, (2), pp. 265–270
[20] Akatsuka K., Ebina Y., Muramatsu M., *ET AL.*: 'Photoelectrochemical properties of alternating multilayer films composed of titania nanosheets and Zn porphyrin', *Langmuir*, 2007, **23**, (12), pp. 6730–6736
[21] Shao F., Zhuo M., Han G., *ET AL.*: 'Synthesis and electrochemical properties study of novel intercalation compound of $KCa_2Nb_3O_{10}$ with cationic methylene blue', *Micro Nano Lett.*, 2013, **8**, (11), pp. 788–791
[22] Han Y.S., Choy J.H.: 'Exfoliation of layered perovskite, $KCa_2Nb_3O_{10}$, into colloidal nanosheets by a novel chemical process', *J. Mater. Chem.*, 2001, **11**, (4), pp. 1277–1282
[23] Xu M., Liang T., Shi M., *ET AL.*: 'Graphene-like two-dimensional materials', *Chem. Rev.*, 2013, **113**, (5), pp. 3766–3798
[24] Tao T., Zhang X., Liu L., *ET AL.*: 'Preparation and electrochemical behaviour study of layered $Bi_2SrTa_2O_9$ with a cationic manganese porphyrin', *IET Micro Nano Lett.*, 2014, **9**, (12), pp. 909–912
[25] Oshima T., Lu D., Ishitani O., *ET AL.*: 'Intercalation of highly dispersed metal nanoclusters into a layered metal oxide for photocatalytic overall water splitting', *Angew. Chem. Int. Ed.*, 2015, **54**, (9), pp. 2698–2702
[26] Zhai Z., Yang X., Xu L., *ET AL.*: 'Novel mesoporous NiO/$HTiNbO_5$ nanohybrids with high visible-light photocatalytic activity and good biocompatibility', *Nanoscale*, 2012, **4**, (2), pp. 547–556
[27] Liu Y.G., Wei C.B., Lv L.L., *ET AL.*: 'A hydrogen peroxide biosensor based on the direct electron transfer of hemoglobin in the nanosheets of exfoliated HNb_3O_8', *J. Solid State Electrochem.*, 2012, **16**, (6), pp. 2211–2216
[28] Zarei-Chaleshtori M., Hosseini M., Edalatpour R., *ET AL.*: 'Photocatalytic decontamination of wastewater with porous material HNb_3O_8', *Microchem. J.*, 2013, **110**, pp. 361–368
[29] Sasaki T., Ebina Y., Tanaka T., *ET AL.*: 'Layer-by-layer assembly of titania nanosheet/polycation composite films', *Chem. Mater.*, 2001, **13**, (12), pp. 4661–4667
[30] Sato M., Abo J., Jin T., *ET AL.*: 'Structure determination of $KLaNb_2O_7$ exhibiting ion exchange ability by X-ray powder diffraction', *Solid State Ion.*, 1992, **51**, (1–2), pp. 85–89
[31] Takano Y., Takayanagi S., Ogawa S., *ET AL.*: 'Superconducting properties of layered perovskite $KCa_2Nb_3O_{10}$ and $KLaNb_2O_7$', *Solid State Commun.*, 1997, **103**, (4), pp. 215–217
[32] Zhang X., Xu J., Wang M., *ET AL.*: 'A manganese porphyrin intercalated lanthanum niobic acid nanocomposite utilized for electrocatalytic oxidation of nitrite', *ECS Electrochem. Lett.*, 2014, **3**, (8), pp. H17–H19
[33] Ida S., Ogata C., Eguchi M., *ET AL.*: 'Photoluminescence of perovskite nanosheets prepared by exfoliation of layered oxides, $K_2Ln_2Ti_3O_{10}$, $KLnNb_2O_7$, and $RbLnTa_2O_7$ (Ln: lanthanide ion)', *J. Am. Chem. Soc.*, 2008, **130**, (22), pp. 7052–7059
[34] Osada M., Sasaki T.: 'Two-dimensional dielectric nanosheets: novel nanoelectronics from nanocrystal building blocks', *Adv. Mater.*, 2012, **24**, (2), pp. 210–228
[35] Guo X., Hou W., Bao G., *ET AL.*: 'Synthesis and characterization of porous chromia-pillared layered lanthanum niobic acid', *Solid State Ion.*, 2006, **177**, (15), pp. 1293–1297
[36] Ma J., Wu J., Zheng J., *ET AL.*: 'Synthesis, characterization and electrochemical behavior of cationic iron porphyrin intercalated into layered niobate', *Microporous Mesoporous Mater.*, 2012, **151**, pp. 325–329
[37] Gopalakrishnan J., Bhat V., Raveau B.: '$A^ILaNb_2O_7$: A new series of layered perovskites exhibiting ion exchange and intercalation behaviour', *Mater. Res. Bull.*, 1987, **22**, (3), pp. 413–417
[38] Liu L., Ma J., Shao F., *ET AL.*: 'A nanostructured hybrid synthesized by the intercalation of CoTMPyP into layered titanate: direct electrochemistry and electrocatalysis', *Electrochem. Commun.*, 2012, **24**, pp. 74–77
[39] Fuerte A., Corma A., Iglesias M., *ET AL.*: 'Approaches to the synthesis of heterogenised metalloporphyrins: application of new materials as electrocatalysts for oxygen reduction', *J. Mol. Catal. A, Chem.*, 2006, **246**, (1), pp. 109–117

doi: 10.1049/mnl.2016.0813